PROCEEDINGS OF THE WORKSHOP BIOSIGNAL 2024, FEBRUARY 28TH - MARCH 1ST, 2024, GÖTTINGEN, GERMANY
10.47952/gro-publ-194

Electrograms in a Cardiac Cell-by-Cell Model

J. Steyer, F. Chegini, T. Starý, M. Potse, M. Weiser, A. Loewe

***Abstract*—Cardiac electrograms are an important tool to study the spread of excitation waves inside the heart, which in turn underlie muscle contraction. Electrograms can be used to analyse the dynamics of these waves, e.g. in fibrotic tissue. In computational models, these analyses can be done with greater detail than during minimally invasive in vivo procedures. Whilst homogenised models have been used to study electrogram genesis, such analyses have not yet been done in cellularly resolved models. Such high resolution may be required to develop a thorough understanding of the mechanisms behind abnormal excitation patterns leading to arrhythmias. In this study, we derived electrograms from an excitation propagation simulation in the Extracellular, Membrane, Intracellular model, which represents these three domains explicitly in the mesh. We studied the effects of the microstructural excitation dynamics on electrogram genesis and morphology. We found that electrograms are sensitive to the myocyte alignment and connectivity, which translates into micro-fractionations in the electrograms.**

***Index Terms*—cardiac electrograms, cell-by-cell model, computational cardiology, excitation wave dynamics**

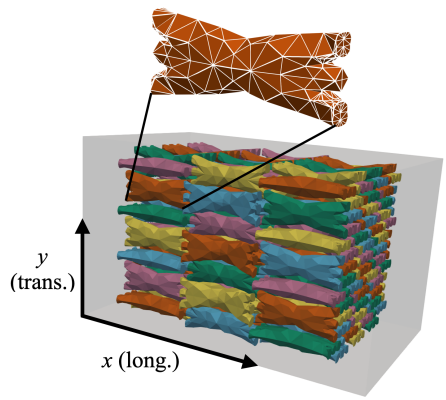

Figure 1: Myocyte alignment embedded in a bath Ω_e (semi-transparent grey). The inset shows a myocyte with its edges in white. Colours discriminate between individual myocytes and do not indicate different electrophysiological properties.

I. Introduction

During minimally invasive surgical procedures, cardiac electrograms (EGMs) are analysed to map the cardiac substrate. From the EGM morphology inferences about the substrate based on pathological excitation patterns can be made. Such pathological excitation dynamics may support arrhythmogenesis. Microstructural excitation patterns play a crucial role in the generation of micro-reentries [1], which in turn may lead to globally arrhythmic excitation patterns. Microstructurally resolved excitation dynamics have not been studied as thoroughly in computational models as excitation dynamics in homogenised models, such as the mono- or bidomain models [2], [3]. Here, we used the novel extracellular-membrane-intracellular (EMI) model, which provides insights into the spread of activation inside and between individual myocytes, to study how these dynamics translate into EGM morphology. In this pilot study, we simulated EGMs resulting from purely longitudinal or transversal excitation, and investigated differences between the two propagation types and differences compared to EGMs measured in vivo or derived from state-of-the-art homogenised simulations.

II. Methods

The EMI model [4] explicitly represents the extracellular medium Ω_e, the cell membrane Γ_m, the intracellular domain $\Omega_\mathrm{i} = \bigcup_j \Omega_j$, where j denotes individual myocyte domains, and the intercalated discs Γ_g that connect the cells. The spatiotemporal behaviour of the intra- and extracellular potentials, ϕ_i and ϕ_e, is governed by

$$\begin{cases} \nabla\cdot(\sigma_\mathrm{i}\nabla\phi_\mathrm{i}) = 0 & \text{in } \Omega_\mathrm{i}, \\ \nabla\cdot(\sigma_\mathrm{e}\nabla\phi_\mathrm{e}) = 0 & \text{in } \Omega_\mathrm{e}, \\ V_\mathrm{m} = \phi_\mathrm{i} - \phi_\mathrm{e} & \text{on } \Gamma_\mathrm{m}, \\ V_\mathrm{g} = \phi_j - \phi_k \quad \text{where} \quad j \neq k & \text{on } \Gamma_\mathrm{g}, \\ C_\mathrm{m}\dot{V}_\mathrm{m} + I_\mathrm{ion} = -\boldsymbol{n}_\mathrm{i}^\mathrm{T}\sigma_\mathrm{i}\nabla\phi_\mathrm{i} = \boldsymbol{n}_\mathrm{e}\sigma_\mathrm{e}\nabla\phi_\mathrm{e} & \text{on } \Gamma_\mathrm{m}, \\ C_\mathrm{m}\dot{V}_\mathrm{g} + I_\mathrm{g} = -\boldsymbol{n}_j^\mathrm{T}\sigma_\mathrm{i}\nabla\phi_j = \boldsymbol{n}_k\sigma_\mathrm{i}\nabla\phi_k & \text{on } \Gamma_\mathrm{g}, \end{cases}$$

where V_m is the membrane voltage between Ω_i and Ω_e, and V_g the voltage between two adjacent cells, Ω_j and Ω_k. $\boldsymbol{n}$ represents the unit outer normal of the respective domain. The scalar conductivities of the intra- and extracellular domains were set to $\sigma_\mathrm{i} = 0.3\,\mathrm{S/m}$ and $\sigma_\mathrm{e} = 2.0\,\mathrm{S/m}$ in this study, while the membrane capacitance was $C_\mathrm{m} = 10^{-4}\,\mathrm{F/m^2}$ as in [5]. For the membrane dynamics, we chose the phenomenological Aliev-Panfilov model [6]. The system was solved using the Kaskade 7 finite element toolbox [7] on a machine equipped with an x86_64 architecture CPU model Intel(R) Xeon(R) E5-2680 v4 and 756 GB RAM. The 3D mesh [8], shown in Fig. 1, has an extension of 400 µm × 240 µm × 240 µm and consists of 507,648 tetrahedral mesh elements. The intracellular domain Ω_i comprises $n_x \times n_y \times n_z = 3 \times 7 \times 7 = 147$ myocytes. The preferential orientation of the myocytes (i.e. the direction of their largest extension), here along the x-axis, is referred to as longitudinal direction. The intercalated disks at which gap junctions are present were located at $x \in \{150, 250\}$ µm, i.e. perpendicular to the x-axis.

J. Steyer, T. Starý, and A. Loewe are with the Institute of Biomedical Engineering, Karlsruhe Institute of Technology (KIT), Karlsruhe, Germany, e-mail: publications@ibt.kit.edu.
F. Chegini and M. Weiser are with Zuse Institute Berlin, Berlin, Germany.
M. Potse is with Liryc, Pessac, France and Inria Centre Bordeaux, Talence, France and Bordeaux Institute of Mathematics, Talence, France

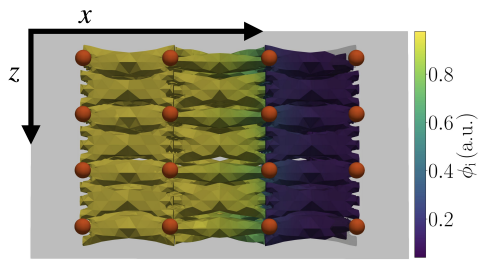

Figure 2: Exemplary snapshot at $t = 2.75\,\mathrm{ms}$ of longitudinal potential propagation with the point electrode positions indicated by red dots.

III. Results

We considered two different types of wave propagation: i) longitudinal propagation by depolarising all leftmost (smallest x) cells and placing a point electrode grid above the mesh in the xz-plane, i.e. with the normal vector of the plane spanned by the electrodes being perpendicular to the propagation direction, see Fig. 2. ii) By depolarising all lowermost myocytes (smallest y), we simulated transversal propagation along the y-axis and measured EGMs with the electrode grid placed in the same position, i.e. with its normal vector parallel to the propagation direction. For these initial stimuli, we used an instantaneous raise of ϕ_i to half its peak value, i.e. 0.5 a.u. Whilst mimicking the topology of clinical electrode grids, the inter-electrode distances are much smaller than those of a real catheter due to the limited size of the computational domain in this pilot study.

Fig. 3 shows the unipolar EGMs, which were directly obtained from $\phi_\mathrm{e}(t)$ values on the nodes where the point electrodes are placed. Most EGMs are either positive or negative, while those in the third column are biphasic. Furthermore, several deflections of different extents can be observed in all EGMs. EGMs taken from the same position and orientation, but with the excitation wave approaching from the bottom and thus, transversal direction, in turn, have more deflections, see Fig. 4. Furthermore, their amplitudes are an order of magnitude smaller than those of the longitudinal propagation.

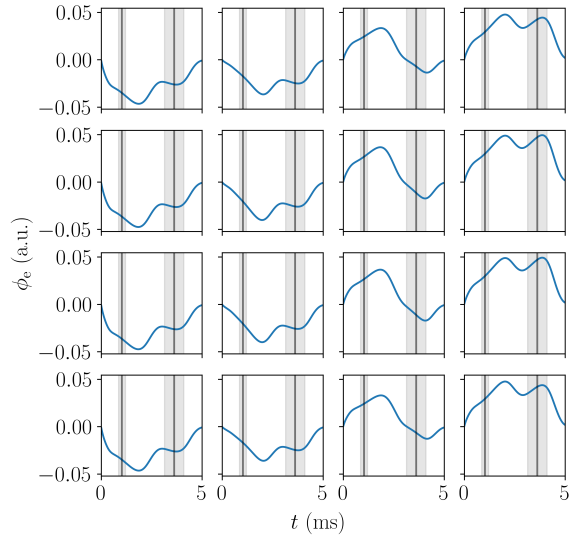

Figure 3: EGMs for the longitudinal propagation shown in the same order as the 4×4 electrode alignment shown in Fig. 2. Dark lines and grey areas indicate the initiation time of excitation propagation in the central and rightmost myocyte column, respectively, i.e. the mean and standard deviation of the local activation times on the intercalated disks.

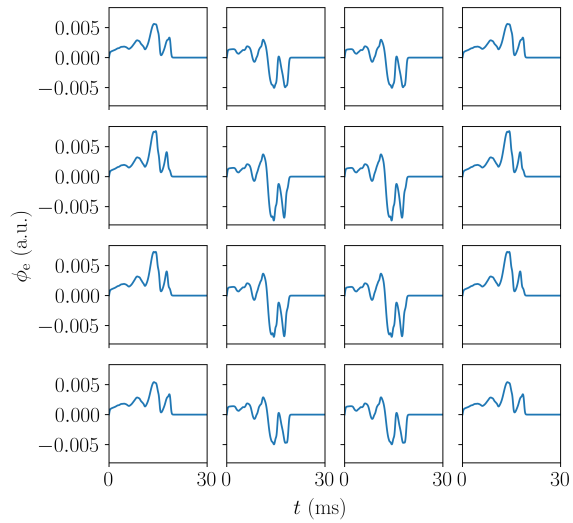

Figure 4: EGMs taken from the electrode positions shown in Fig. 2 but with a transversally propagating wave.

IV. Discussion and Conclusion

Even though the electrodes were placed at the same locations for both propagation types, the wave approached the electrode mesh (xz-)plane spanned by them differently. The longitudinal wave travels perpendicular to this plane's normal vector while the transversal wave approaches the plane frontally. The first two columns in Fig. 3 show only negative EGMs. This morphology results from the beginning of the simulation, where only already depolarised or departing waves are sensed by the corresponding electrodes. In the third column, we can see approximately symmetric EGMs, with a pronounced maximum, followed by a similarly large minimum. This occurs because these electrodes are the only ones under which the wave actually travels from the left to the right. These biphasic EGMs are equivalent to the symmetric EGMs observed clinically [9] and reproduced in simulations with homogenised models [10], [11] for plane wave propagation, where the maximum corresponds to the approaching and the minimum to the departing wave. Finally, the last column has positive EGMs only as the excitation approaches these electrodes throughout the simulation and then hits the boundary of the computational domain. The local activation times for the initiation of excitation propagation in the central and rightmost myocyte layers (Fig. 2) match with the aforementioned translation of excitation dynamics into the EGM morphology. Specifically, this means that there are positive slopes for departing waves and negative slopes for incoming excitation, relative to the electrode positions at these

activation times.

For the transversal excitation propagation, the amplitudes of the EGMs obtained by the transversal propagation are strongly reduced (Fig. 4), which can be explained by the overall slower wave propagation. Even though the propagation within the myocytes themselves is isotropic, the effective transversal propagation speed is lower due to the longer and more sinuous path that transverse propagation has to follow, as the intercalated disks only connect cells in longitudinal direction. These propagation delays have different extents, which in turn allow multimodal activation along this direction, meaning that the depolarisation of myocytes along this direction is not necessarily simultaneous. This multimodality translates into the EGMs and explains why there are more deflections than for the longitudinal propagation, which is different from what we would expect from homogenised models [2]. A frontally approaching excitation wave would be measured as a large peak without any negative values in $\phi_\mathrm{e}(t)$, as the multimodality in activation would not be present due to homogenisation, resulting in an approximately uniform plane wave. The fact that the two central columns show both minima and maxima, while the two outer columns are positive only, can be explained by a faster excitation spread in the middle myocyte layer (i.e. where $x \in [150, 250]\,\mu\mathrm{m}$), which in turn is due to an increased inter-myocyte proximity of this segment along the transversal direction. This allows for both approaching and departing waves relative to these electrodes to be recorded simultaneously. The positive outer electrograms reflect this as well, since they only sense approaching waves.

This study is a first example of how even healthy myocyte alignments (i.e. no fibrosis or blocks introduced to the mesh) cause micro-fractionation in the EGM, which would not be observed in homogenised models, e.g. [2]. Our setup, however, has several restrictions. First of all, representing only 147 myocytes, the tissue patch we are looking at is very small and consequently, the amplitudes of the EGMs measured here do not reflect what would be measured clinically, where the excitation propagation of the whole heart contributes to the EGMs to different extents, depending on the distance between electrode and excitation source. In addition, the parameter set for future studies needs to be adjusted and combined with refined meshes as the conduction velocity is one order of magnitude smaller than what we would expect in healthy cardiac tissue [12]. In order to represent the myocytes more realistically, future studies will have to consider subcellular conduction anisotropy caused e.g. by the cell organelles, such as the nucleus. Furthermore, we used a repetitive mesh in which the intercalated disks are aligned on yz planes. A more irregular mesh is needed to realistically represent the myocyte intertwining.

This study provides a base for sophisticated simulations demonstrating the effect of tissue pathologies on EGM properties. Such studies could help, for example, to improve diagnosis, targeted treatment, and the design of catheter electrodes.

Acknowledgment

This work was supported by the European High-Performance Computing Joint Undertaking EuroHPC under grant agreement No 955495 (MICROCARD) co-funded by the Horizon 2020 programme of the European Union (EU), the German Federal Ministry of Education and Research and the French National Research Agency ANR.

References

[1] J. M. T. de Bakker, R. Coronel, S. Tasseron *et al.*, "Ventricular tachyrdia in the infarcted, langendorff-perfused human heart: Role of the arrangement of surviving cardiac fibers," *Journal of the American College of Cardiology*, vol. **15**, no. 7, pp. 1594–1607, 1990. [Online]. Available: https://doi.org/10.1016/0735-1097(90)92832-M

[2] G. Plank, A. Loewe, A. Neic *et al.*, "The openCARP simulation environment for cardiac electrophysiology." *Computer Methods and Programs in Biomedicine*, vol. **208**, p. 106223, 6 2021. [Online]. Available: http://doi.org/10.1016/j.cmpb.2021.106223

[3] J. Sundnes, B. Nielsen, K. Mardal *et al.*, "On the computational complexity of the bidomain and the monodomain models of electrophysiology." *Annals of Biomedical Engineering*, vol. **34**, no. 7, pp. 1088–1079, 2006. [Online]. Available: doi.org/10.1007/s10439-006-9082-z

[4] A. Tveito, K. Mardal, and M. Rognes, *Modeling Excitable Tissue: The EMI Framework*, ser. Simula Springer Briefs on Computing. Springer International Publishing, 2020. [Online]. Available: https://doi.org/10.1007/978-3-030-61157-6

[5] F. Chegini, T. Steinke, and M. Weiser, "Efficient adaptivity for simulating cardiac electrophysiology with spectral deferred correction methods," 2023. [Online]. Available: https://doi.org/10.48550/arXiv.2311.07206

[6] R. R. Aliev and A. V. Panfilov, "A simple two-variable model of cardiac excitation," *Chaos, Solitons & Fractals*, vol. **7**, no. 3, pp. 293–301, 1996. [Online]. Available: https://doi.org/10.1016/0960-0779(95)00089-5

[7] M. Weiser and F. Chegini, "Higher-order time integration using spectral deferred correction method (SDC) in a cell by cell discretization of cardiac excitation," 2022. [Online]. Available: https://doi.org/10.35097/716

[8] M. Potse, L. Cirrottola, and A. Froehly, "A practical algorithm to build geometric models of cardiac muscle structure," in *8th European Congress on Computational Methods in Applied Sciences and Engineering*, Oslo, Norway, Jun. 2022. [Online]. Available: https://doi.org/10.23967/eccomas.2022.027

[9] J. M. T. de Bakker, "Electrogram recording and analyzing techniques to optimize selection of target sites for ablation of cardiac arrhythmias," *Pacing and Clinical Electrophysiology*, vol. **42**, no. 12, pp. 1503–1516, 2019. [Online]. Available: https://doi.org/10.1111/pace.13817

[10] J. Sánchez and A. Loewe, "A review of healthy and fibrotic myocardium microstructure modeling and corresponding intracardiac electrograms," *Frontiers in Physiology*, vol. **13**, 2022. [Online]. Available: https://doi.org/10.3389/fphys.2022.908069

[11] J. Steyer, L. P. M. Diaz, L. A. Unger *et al.*, "Simulated excitation patterns in the atria and their corresponding electrograms," in *Functional Imaging and Modeling of the Heart*. Cham: Springer Nature Switzerland, 2023, pp. 204–212. [Online]. Available: https://doi.org/10.1007/978-3-031-35302-4_21

[12] B. Verma, T. Oesterlein, Loewe *et al.*, "Regional conduction velocity calculation from clinical multichannel electrograms in human atria," vol. **92**. Elsevier, 1 2018, pp. 188–196. [Online]. Available: https://doi.org/10.1016/j.compbiomed.2017.11.017